Activity-regulated RNA editing in select neuronal subfields in hippocampus

Ales Balik[1,2], Andrew C. Penn[1], Zsofia Nemoda[1] and Ingo H. Greger[1,*]

[1]Neurobiology Division, MRC Laboratory of Molecular Biology, Cambridge, CB2 0QH, UK and [2]Institute of Physiology, ASCR v.v.i., 142 20 Prague, Czech Republic

ABSTRACT

RNA editing by adensosine deaminases is a widespread mechanism to alter genetic information in metazoa. In addition to modifications in non-coding regions, editing contributes to diversification of protein function, in analogy to alternative splicing. However, although splicing programs respond to external signals, facilitating fine tuning and homeostasis of cellular functions, a similar regulation has not been described for RNA editing. Here, we show that the AMPA receptor R/G editing site is dynamically regulated in the hippocampus in response to activity. These changes are bi-directional, reversible and correlate with levels of the editase Adar2. This regulation is observed in the CA1 hippocampal subfield but not in CA3 and is thus subfield/celltype-specific. Moreover, alternative splicing of the flip/flop cassette downstream of the R/G site is closely linked to the editing state, which is regulated by Ca^{2+}. Our data show that A-to-I RNA editing has the capacity to tune protein function in response to external stimuli.

INTRODUCTION

Adenosine-to-inosine (A-to-I) RNA editing is a unique mechanism to expand and diversify functions of the protein repertoire (1). Select adenosines in pre-mRNA are targeted by enzymatic deamination to inosine, which is read as guanosine during translation. Editing by adenosine deaminases acting on RNA (Adars) requires complex RNA secondary structures, which in most cases are formed between the editing-site region and a complementary inverted repeat sequence (1). In addition to altering reading frames, A-to-I editing targets non-coding regions, which impacts on splicing and RNA metabolism (2–4).

A-to-I editing targets are abundant in nervous systems where Adar levels and in turn the concentration of inosine-containing RNA are highest (5–7). Proteins involved in synaptic transmission, including ion channels and G-protein coupled receptors, are recoded at strategic positions in both vertebrates and invertebrates (6,8,9). These changes result in profound alterations in neuronal signaling and can give rise to severe neurological disorders when mis-regulated (10,11). A dramatic example is provided by alpha-amino-3-hydroxy-5-methyl-4-isoxazolepropionic acid (AMPA)-type ionotropic glutamate receptors, the main mediators of fast excitatory neurotransmission (12). Here, editing targets the channel pore and the ligand-binding domain (LBD) of the receptor (13). Editing at the Q/R site in the pore affects ion selectivity (rendering the edited channel Ca^{2+} impermeable) and subunit assembly (14,15). Q/R editing is essential for survival of the organism and is compromised in a variety of neurological disorders, including epilepsy (10,16). In contrast, editing at the R/G site alters the speed of recovery from a non-conducting, desensitized state and thereby influences how the receptor decodes trains of incoming action potentials (17). Like the Q/R site, R/G editing also modulates receptor assembly by limiting the capacity of GluA2 to form homomeric channels in the endoplasmic reticulum (ER) and thereby promotes the formation of (functionally diverse) AMPAR heterotetramers (18). Together, editing of the GluA2 subunit has a profound impact on AMPAR-mediated neurotransmission at various levels.

Alternative splicing can be subject to regulation by external stimuli, including hormones and cell depolarization, thus providing adaptive means to orchestrate protein diversification (19). In many cases, this involves Ca^{2+} signaling. A well-described example is the splicing regulation of the STREX exon in BK potassium channel transcripts via activation of Ca^{2+}/calmodulin kinase IV (20). In the case of AMPA receptors, alternative splicing of the

mutually exclusive flip/flop (i/o) exons (encoding residues within the LBD dimer interface) responds to Ca^{2+} through L-type Ca^{2+} channels (21). The i/o cassette lies immediately downstream of the R/G site and similarly impacts on AMPAR biogenesis and gating (22–25). Although Adar1 can be induced under specific pathological conditions [e.g. response to viral infection (26)], whether editing by Adars could also be regulated by physiological cues is currently unclear.

Here, we report that RNA editing by Adar2 responds to activity in an intact neuronal circuit. This regulation is cell-type-specific, bi-directional and involves Ca^{2+} influx. Moreover, not all editing sites respond to the same degree, which will be linked to features of the RNA substrate and Adar selectivity. The AMPAR GluA2 R/G site shows bi-directional regulation, which is reversible. R/G editing correlates with Adar2 mRNA levels, which are elevated under high-activity conditions but reduced when activity is lowered. In addition, editing is closely correlated to alternative splicing at the alternative i/o exons, positioned immediately downstream of the R/G site. Recoding this editing site in response to external cues will shape AMPAR biogenesis and kinetics and is thereby expected to tune excitatory neurotransmission.

MATERIALS AND METHODS

Slice preparation and treatments

All procedures were carried out in accordance with UK Home Office regulations. Sprague–Dawley rat hippocampi were dissected from pups (postnatal age 5 days) in a sucrose-modified Gey's balanced salt solution, which was (in mM): sucrose (175), NaCl (50), KCl (2.5) Na_2HPO_4 (0.85), KH_2PO_4 (0.66), $MgSO_4$ (0.28), $MgCl_2$ (2) $CaCl_2$ (0.5), glucose (25) and $10\,\mu g/ml$ phenol red (~330 mOsm, pH 7.3). Transverse hippocampal slices (350-μm thick) were cultured using the roller-tube method on collagen-coated coverslips in an incubator at $36°C$ without humidity or CO_2 control (27) or using an interface method. Culture medium contained (all from GIBCO) 50% Basal Medium Eagles, 25% Hank's balanced salt solution, 25% heat-inactivated horse serum, 1 mM L-Glutamine and 6.5 g/l dextrose (320 mOsm). At 3–4 days *in vitro*, slices were fed with culture medium supplemented with 1 μM each cytosine β-D-arabinofuranoside, 5-fluoro-2′-deoxyuridine and uridine (Sigma). Slices were fed the following day and twice weekly thereafter (without antimitotics).

Slices were cultured for at least 3 weeks prior to treatments. For treatments, slices were fed with culture medium containing tetrodotoxin (TTX, 1 μM), bicuculline (BIC, 20 μM), Nifedipine (NIF, 100 μM), Carbachol (Carb 20 μM), kainate (10 μM) or no drug (CTRL). Slices were returned to the incubator for a duration of 48 h, after which they were dissected for molecular biology.

Acute rat brain tissue was dissected in a phosphate buffer salt solution (PBS, pH 7.2). Transverse hippocampal slices (400 μm) were cut using a tissue chopper (McIllwain). Slices were collected in ice-cold PBS and hippocampal subfields were dissected under a dissection microscope (Zeiss) and RNA extracted as described below.

Molecular biology

RNA was extracted from tissue with Trizol according to the manufacturer's instructions (Invitrogen). The nucleic acid pellet was re-suspended in RNase-free water, treated with DNase I and used as template for random primed cDNA synthesis catalyzed by Moloney Murine Leukemia Virus (MMLV) reverse transcriptase (Promega). Polymerase chain reaction (PCR) was conducted with *Thermus aquaticus* (*Taq*) polymerase (Invitrogen) using standard protocols. Amplicons were either sequenced directly (Geneservice, UK) or cloned into pGEM T-Easy vector (Promega) and transformed into *Escherichia coli* for individual clone sequencing (GATC, Germany). Peak heights in sequence chromatograms were quantified using PeakPicker software (28). To quantify splicing, the mean of the first five different base positions for the alternatively spliced exon were used. To calculate simultaneous 95% confidence intervals (CIs) for the multinomial subunit variant proportions in Figure 2C, we used the method of Goodman (29).

For analysis of *Adar2* splicing (and thus self-editing), the PCR amplicon of the ROI was run on agarose gels and post-stained with ethidium bromide. Quantifications were made on gel images by measuring band peak intensities using ImageJ (NIH).

Quantitative real-time PCR

Alternations in ADARs expression levels were determined by real-time PCR. Pre-designed TaqMan assays (Adar1 Rn00508006_m1, Adar2 Rn00563671_ml, GAPD 4352338E; β-2-microglobulin Rn00560865_m1; ABI) were used and validated according to manufacture protocols. Reactions were run on the Rotor-Gene 6000 and analyzed with Rotor-Gene Software1.7 (Qiagen).

Bioinformatics

The R/G editing substrates of GluA2–4 published for rat (17) were used as a Basic Local Alignment Search Tool (BLAST) or BLAST-Like Alignment Tool (BLAT) search queries to indentify homologues from the online Ensembl and Pre-Ensembl vertebrate assemblies (30–32). Species with diploid genomes were selected to represent major taxonomic branches in vertebrate evolution. Shark sequence was retrieved from the whole genome shotgun sequence database on the Institute of Molecular and Cell Biology server (33). The sequence coordinates and associated information are documented in Supplementary Table S1. The subunit identity of the editing substrates (and the adjacent translated exon 13 sequence) for the paralogs was confirmed from pairwise alignment output information using Clustalw2 (www.ebi.ac.uk/Tools/msa/clustalw2/, data not shown). Sequences were then aligned using Multiple Alignment based on Fast Fourier Transform (MAFFT) by iterative refinement with pairwise alignment information [G-INS-i; Version 6.903; (34)]. Sequence similarity was calculated for each paralog and data output from the PLOTCON application

in European Molecular Biology Open Software Suite (EMBOSS) using the EDNA scoring matrix and a window size of 1. The γ-centroid consensus structure was predicted from the alignment using CentroidAlifold with a default inference engine [Version 0.0.9; (35)]. The common structure was superimposed onto the rat or consensus pre-mRNA sequence and visualized with Visualization Applet for RNA (VARNA) [Version 3.8; (36)]. The posteriors were used to plot the probabilities of base pairs shown in the consensus structure. To predict the strength of the exon 13 splice donor before and after editing, we used an algorithm developed by C. Burge, available at: http://genes.mit.edu/burgelab/maxent/Xmaxentscan_scoreseq.html.

Data analysis

Most statistical comparisons were performed using non-parametric methods in Prism 5.0b or Instat 3.1a (Graphpad Software Inc). Other statistical analyses were performed using R 2.81 (http://www.r-project.org/). Graphical presentation of data was carried out in Excel (Microsoft).

RESULTS

Activity-mediated RNA editing in CA1 neurons

RNA editing in the LBD plays a strategic role in AMPAR signaling–it influences channel biogenesis and gating kinetics (17,18,24,37). To address whether editing is regulated by external signals, we utilized a physiologically relevant system, organotypic slice cultures from rat hippocampus (27). This tri-synaptic circuitry comprises anatomically and functionally diverse neuronal subfields (Figure 1A), which are connected by defined inputs (38). A key advantage of this morphological segregation is that distinct principal neuron types can be studied selectively [Figure 1A; right panel, see also reference (21)].

To modulate activity, we chronically treated slices (48 h) with the sodium channel inhibitor TTX or with the GABA-A channel blocker BIC. TTX will silence the network by inhibiting action potential firing (by blocking Na^+ channels), whereas BIC increases activity by blocking GABA-A receptor-mediated neuronal inhibition. Neurons reset their response gain homeostatically in response to chronic changes in activity (39,40). We find that upon TTX treatment, R/G editing of GluA2 diminishes significantly. In contrast, heightened activity after chronic BIC shows the opposite trend: enhanced editing, thus revealing bi-directional control of the GluA2 R/G site (Figure 1B–D). This was corroborated by consecutive drug treatments: where TTX followed by BIC elevated editing levels to a BIC pattern and vice versa (Supplementary Figure S1A). GluA2 R/G editing is thus reversible.

Notably, activity-mediated editing is also subfield- and substrate-specific. CA3 neurons, a morphologically and functionally distinct group (Figure 1A), did not respond to the drug treatments (Figure 1E). In fact, R/G editing is significantly higher in CA3 than in CA1 in untreated control slices (Figure 1F), which is seen also in RNA harvested from acutely dissected rat hippocampus

(Supplementary Figure S2). Chronic TTX did not lower editing levels in CA3 suggesting that reprogramming is subfield/celltype-specific. In addition, substrate specificity is apparent as bi-directional editing is seen for GluA2 and GluA4 (data not shown) transcripts but not to the same extent for the closely related GluA3 paralog (see below). The time course for editing changes at the R/G site in response to TTX had a half-life of ∼11 h (Figure 2A), revealing a gradual, cumulative change that was apparent at the earliest time point (i.e. 6 h post-TTX).

Beyond activity elevation by BIC, we found that physiologically more realistic manipulations altered RNA processing in the LBD. Inducing gamma oscillations with the cholinergic agonist Carbachol (48 h Carb) (41) also resulted in a trend-wise increase in levels of GluA2 R/G editing and in a significant elevation of flip exon inclusion (Supplementary Figure S3). Similarly, raising activity with a partial glutamate receptor agonist, the neurotoxin kainate, mimicked mRNA patterns obtained after chronic BIC treatments (data not shown). We have shown recently that i/o splicing is regulated by activity and that this requires Ca^{2+} influx through L-type Ca^{2+} channels (which are expressed abundantly in CA1 neurons) (21). Blocking L-type Ca^{2+} channels with Nifedipine (NIF) significantly reduced R/G editing (Supplementary Figure S1B), suggesting that the editing machinery responds to Ca^{2+} fluctuations. Taken together, R/G editing is dynamically regulated by neuronal activity, which is linked to Ca^{2+} influx.

R/G editing is linked to flip/flop splicing

The segregation of editing between subfields adds to previously described differences in alternative (i/o) splicing: flip expression dominates in rodent CA3, whereas flop prevails in CA1 (Figure 1A) (37). This strict segregation of alternative RNA processing between adjacent (but functionally distinct) brain regions is unique, but the underlying regulation is unknown. The R/G site locates to the end of exon 13 and is embedded in the splice donor upstream of the alternative i/o splice acceptors (Figure 1B). Conversion of the editing-site A-to-I is predicted to weaken the splice donor in exon 13 (score: unedited = 8.23; edited = 5.37; see 'Materials and Methods' section) and may thereby affect the choice between alternative 3' splice acceptor sites. This prediction did not hold in HEK293 cells expressing minigene reporters of exons 13–16 encoding either an A or a G at the editing site position (data not shown). Co-transfection of rat Adar2b with the wild-type minigene reporter caused erroneous editing at the neighboring adenine and this approach was not pursued further in this study.

However, GluA2 R/G editing significantly correlated with flip exon selection in CA1 neural tissue, where a close to linear relationship between editing to G and flip-exon inclusion was evident ($r = 0.68$, $P = 0.0001$, Spearman's rank test; Figure 2B; Supplementary Figures S2 and S4A). As editing occurs before splicing, this implies that altering position −2 in the splice donor (the editing site; Figure 1B) could impact on alternative splicing to facilitate inclusion of the downstream flip exon (exon 15).
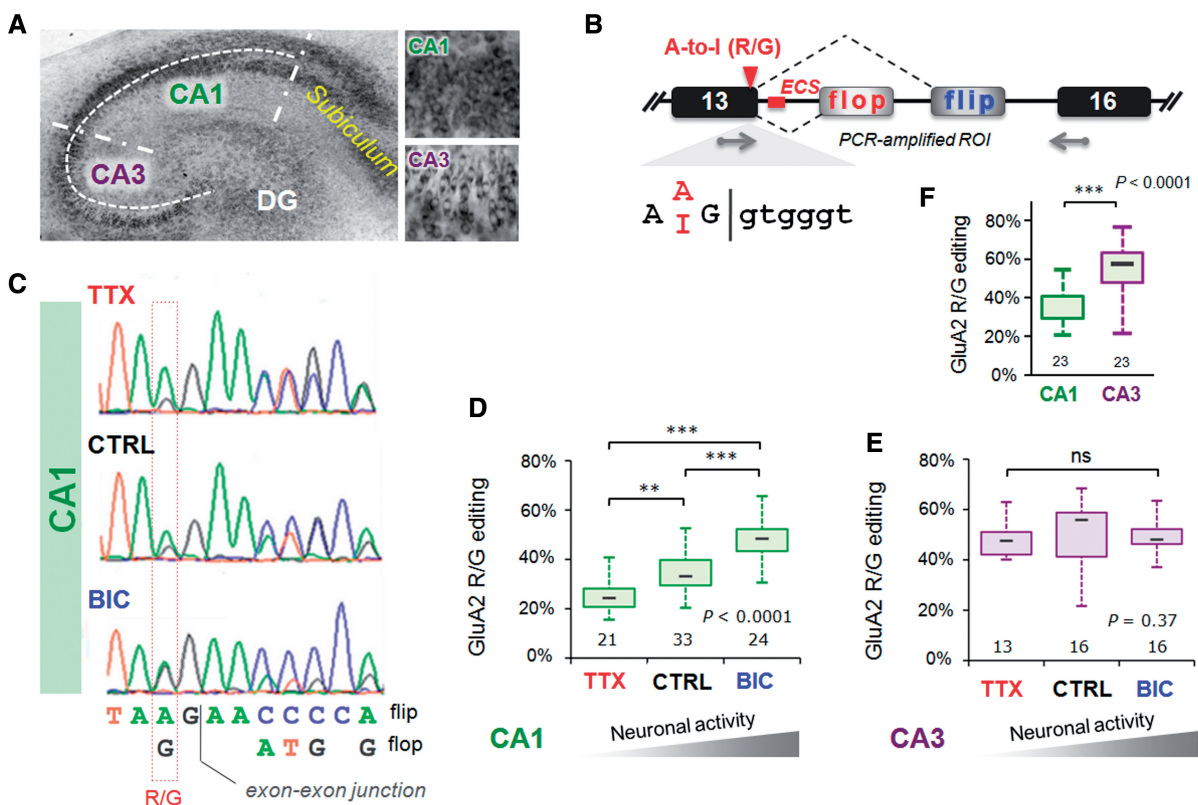
Figure 1. Activity-dependent changes in GluA2 R/G editing localized to hippocampal CA1. (**A**) Nissl stain of an organotypic culture of a transverse hippocampal slice cultured for 3 weeks. The major subfields of the trisynaptic circuit are annotated: CA1, CA3 and the dentate gyrus. Right top and bottom show close-up images of CA1 and CA3 cells respectively. (**B**) Schematic illustrating the *Gria2* locus encompassing exons 13–16; the region of interest (ROI), encodes segment 2 of the ligand-binding domain, the alternatively spliced i/o exons and the A/I RNA editing site, where arginine (R) is recoded to a glycine (G). The editing complementary sequence (ECS) forms a highly conserved pre-mRNA secondary structure encompassing the splice site (see Figure 4A). (**C**) Sequence traces show part of the ROI including the A/I editing site and the exon–exon junction between exon 13 and the flip/flop exon. Changes in *GluA2* editing and splicing from mRNA extracted from CA1 tissue after 48 h TTX or BIC treatments. CTRL treatment represents mock feeding without drugs. (**D**) Quantification of the peak heights in CA1 sequence chromatograms is summarized in box and whisker plots. The plot shows levels of GluA2 R/G editing as a fraction of total subunit mRNA for the different drug treatments. The median is represented by a gray line. The box and whiskers show the interquartile range (25–75%) and the total range (min–max) of the data, respectively. The number at the base of each plot is the number of slices. The *P*-value is derived from the Kruskal–Wallis test statistic and the asterisks summarize the results of Dunn's post-tests: **$P < 0.01$, ***$P < 0.001$. (**E**) As in Figure 1D but for mRNA extracted from micro-dissected CA3 tissue after 48 h treatments with TTX or BIC. Editing and splicing of *GluA2* are invariant across drug treatments. (**F**) Box and whisker plots summarizing GluA2 R/G editing levels between subfields (CA1 and CA3) determined from peak height ratios. The *P*-value is derived from the Mann–Whitney *U*-statistic, ***$P < 0.0001$.

Furthermore, analysis of individual clones revealed that the distinction between drug treatments apparently resulted from a shift in the balance of edited-flip (i-G) and unedited-flop variants (o-R). Specifically, BIC boosted edited-flip (i-G) representation, whereas unedited flop variants (o-R) prevailed after chronic TTX. This coupling between editing and splicing was also apparent in CA3 tissue and for the GluA3 R/G site, although neither responded to changes in activity (Figures 1E and 4B; Supplementary Figure S4B). These findings suggest a potential mechanistic link between R/G editing and downstream splice site choice (Figure 2B, lower panel), which extends earlier data where editing was reported to repress splicing of the adjacent flop exon in a reporter system (42).

Adar levels fluctuate in response to neural activity

A-to-I editing is catalyzed by editase (Adar) dimers (43,44); individual substrates are recognized by the catalytically active Adar1 or Adar2, or by a combination of the two enzymes. Editing at the GluA2 R/G site is mediated mostly by Adar2, whereas both enzymes target the R/G site in GluA3 (45,46). Adar2 is expressed at higher levels in subfield CA3 than in CA1 (~3-fold in adult rat hippocampus). This was not the case for Adar1, which is expressed homogeneously across hippocampal subfields (Supplementary Figure S5A). The more prominent level of Adar2 in CA3 is also evident with *in situ* hybridization data of mouse hippocampus (Supplementary Figure S5B) (47). Related to this Adar2 expression profile, GluA2 R/G editing is consistently higher in CA3, in both acutely dissected and in organotypic hippocampal slices (Figure 1F and Supplementary Figure S2).

This raises the question as to whether changes in Adar2 expression could contribute to the changes in GluA2 R/G editing in CA1. Adar2 expression is under negative feedback control and has been shown to fluctuate in
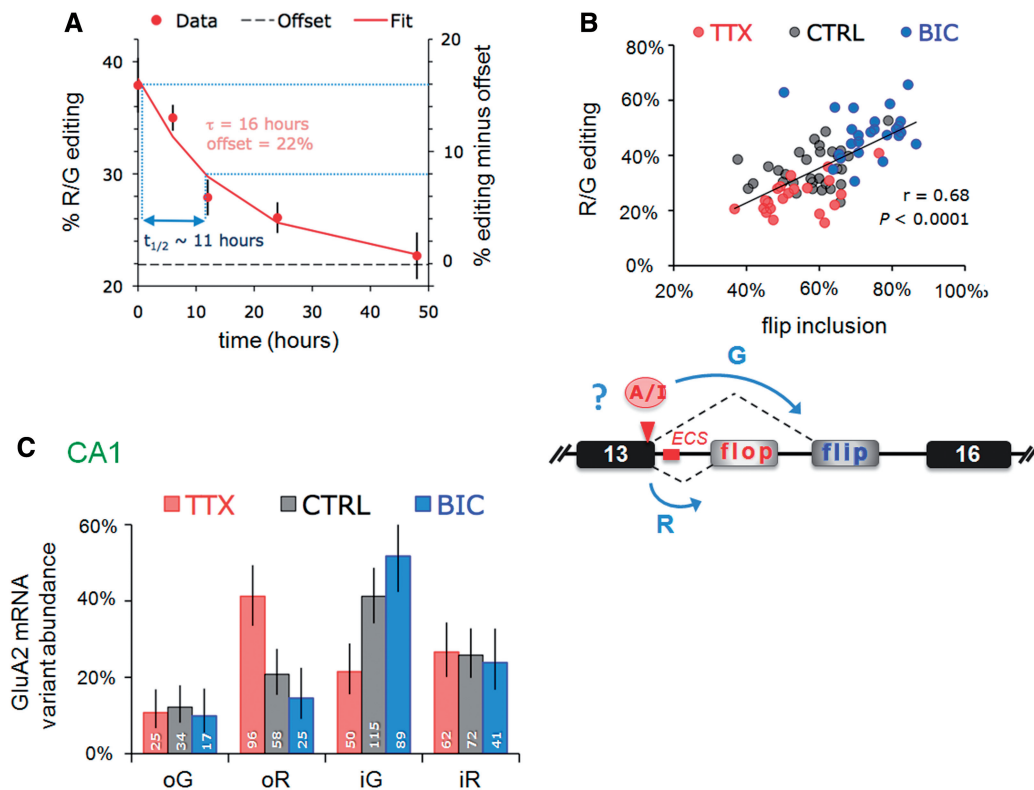
Figure 2. Changes in the expression of a subset of GluA2 mRNA variants underlie correlated editing and splicing. (**A**) Time course of GluA2 R/G editing changes in response to TTX. Slices were harvested 0, 6, 12, 24 and 48 h post-TTX. The sample size was eight to nine slices/time point. The amount of edited mRNA as a percentage of total GluA2 was determined from peak measurements of sequence traces. Data points were fit with a single exponential ($y = Ae^{-\tau/t} + c$). A half-life ($t_{1/2}$) of 16 h was determined from the time constant (τ) using the equation: $t_{1/2} = \tau \cdot -\ln(0.5)$. (**B**) Top: the editing and flip/flop splicing determined from sequence chromatograms are plotted for each slice. Data points for each treatment are represented by different colors: red = TTX; black = CTRL; blue = BIC. The correlation coefficient (r) and P-values are determined by Spearman's rank test on the entire data set. Bottom: schematic illustrating the Gria2 locus and a potential interaction between A-to-I editing and pre-mRNA splicing (blue arrows). (**C**) PCR products were ligated into a bacterial expression vector, transformed into *E. coli* and editing/splice-variant status of individual clones was identified by DNA sequencing. The bar graphs show the proportions determined from the weighted-mean of clone counts from 7, 8 and 7 slices for TTX, CTRL and BIC treatments, respectively. Total number of clones were 270, 335 and 256 for TTX, CTRL and BIC treatments, respectively. Error bars represent 95% CI for proportions. Data for each treatment are represented by different colors: red = TTX; gray = CTRL; blue = BIC. The number at the base of each column represents the number of clones.

response to external stimuli (48–50). In our system, *Adar2* levels indeed fluctuated between activity regimes: relative to control, *Adar2* mRNA levels were elevated under heightened activity (BIC) but were reduced under network silence (TTX) (Figure 3A). *Adar2* levels also responded to Ca^{2+} perturbations, as expression similarly diminished after chronic NIF treatment (Figure 3A), which explains the lowered levels of GluA2 R/G editing post-NIF (Supplementary Figure S1B). Moreover, a relationship between *Adar2* expression levels and the extent of editing at the GluA2 R/G site was apparent ($r = 0.60$, $P = 0.0011$; Spearman's rank test) (Figure 3B). Therefore, regulation of enzyme levels could contribute to the bi-directional recoding described above.

Rodent *Adar2* levels are under negative feedback control via self-editing, resulting in inclusion of a 47-nt segment in exon 5 (Figure 3C), which gives rise to truncated, non-functional Adar2 protein (49). Editing of the *Adar2* transcript could therefore be another hallmark of Adar2 editase activity. Consistent with this, we detected higher levels of self-edited *Adar2* in CA3, relative to CA1, at

steady-state (data not shown). Bi-directional shifts in *Adar2* self-editing were also apparent in CA1 in response to the activity regimes; i.e. greater levels of self-editing were evident under heightened activity (Figure 3C and D), where *Adar2* levels are upregulated (Figure 3A). Together, this implies a dynamic, L-type Ca^{2+} channel-mediated regulation of Adar2 expression in the hippocampus.

The GluA2 R/G site is prone to dynamic regulation

In invertebrates, Adar deletion results in severe behavioral deficits [e.g. (8)]. A relationship between *Adar2* levels and editing has been described also for the GluA2 Q/R site under severe pathological conditions. These include motor neurons in amyotrophic lateral sclerosis (ALS) (51,52) and CA1 hippocampus under experimentally-induced ischemia (53). The Q/R-editing state of mRNA was not altered under our conditions. This efficiently edited site is saturated in control slices, which together with preferential splicing of the Q/R-edited pre-mRNA could make Adar2 downregulation in TTX insufficient to impact on the Q/R site (Supplementary Table S2)
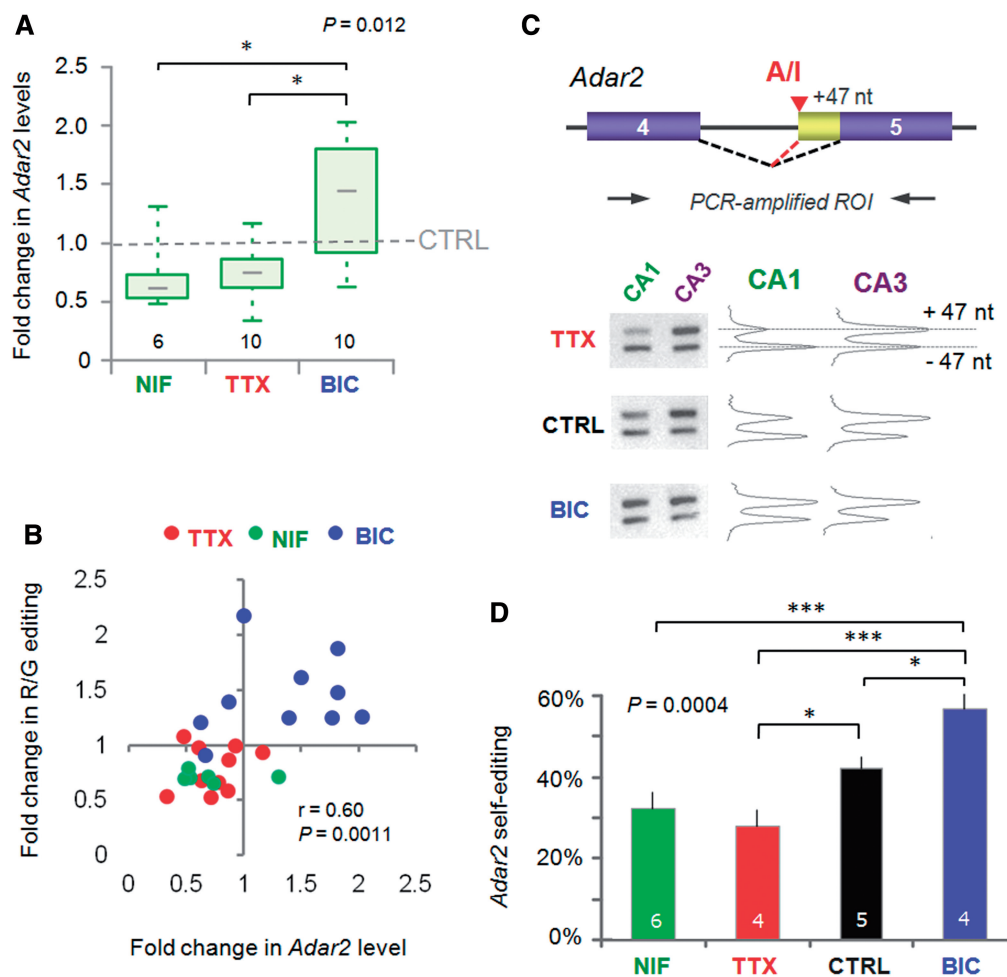
Figure 3. RNA editing at the R/G site is correlated with altered mRNA levels and self-editing of the deaminase *Adar2*. (**A**) The fold change in CA1 mRNA levels of *Adar2* for (48 h) drug treatments compared with the mean of CTRL samples from the same PCR runs. *Adar2* expression was measured by real-time PCR using Taqman chemistry (FAM) and normalized to the endogenous house-keeping gene *Gapdh* (VIC). The graph summarizes data from four real-time PCR runs. The $\Delta\Delta C_T$ method was used for analysis. By validation, standard curves run for primer-probe sets gave primer efficiencies >90%. Almost identical results were obtained using the β-2-microglobulin as a house keeping gene. The *P*-values are derived from the Kruskall–Wallis ANOVA test statistic and the asterices summarize the results of Dunn's post-tests: *$P < 0.05$. (**B**) Changes in GluA2 R/G editing are positively correlated with changes in *Adar2* expression. The fold change in GluA2 R/G editing is plotted against the fold change in mRNA levels of *Adar2* for the same CA1 samples after 48 h drug treatments. Both editing and *Gapdh*-normalized *Adar2* expression are compared with the mean of CTRL samples from the same PCR runs. Data points for each treatment are represented by different colors: red = TTX; blue = BIC; green = NIF. The correlation coefficient (*r*) and *P*-values are determined by Spearman's rank test on the entire data set. (**C**) Neuronal activity triggers Adar2 auto-regulation by self-editing. Adar2 edits its own pre-mRNA in intron 2 to generate a new 3′ splice site to extend the second coding exon by 47 nt (top). The resulting frameshift leads to premature stop codon and a non-functional truncated protein. Thereby, Adar2 self-editing represents auto-regulation of its own expression by negative feedback. This is assayed by PCR amplification of the ROI (top) and separation of the fragments by gel electrophoresis (bottom left). Gel images were quantified using ImageJ software (NIH) (bottom right). (**D**) Plot summarizing the results of the quantification for +47 nt inclusion and thus self-editing for the different treatments. After 48 h activity deprivation with TTX and NIF, self-editing is lower, whereas increased activity has the opposite effect. The *P*-value is derived from the ANOVA test statistic and the asterices summarize the results of Student–Newman–Keuls post-tests: *$P < 0.05$, ***$P < 0.001$.

(45,54). In addition, changes to chronic treatments at other editing sites, including GluK2 Kainate receptor sites (Y/C, I/V, Q/R), the 5HT-2C serotonin receptor and the GluA3 R/G site (see above), were relatively modest (Supplementary Table S2). This heterogeneity could relate to the baseline efficacy of editing at a given RNA substrate (such as the high editing efficacy of the Q/R site), or to Adar substrate-specificity. For example, the intronic hotspots in *GRIA2* intron 11: hotspot 1 (the +60 site), primarily an Adar1 target (45), is unaffected by the activity regimes, whereas editing of hotspot 2 (+262) is

Adar2-mediated and is responsive [Supplementary Table S2; (54)]. Of note, we cannot exclude the possibility that other substrate-specific factors (e.g. splicing efficiency, activators/inhibitors) also contribute to differences in the activity regulation of the different editing sites.

The AMPAR R/G substrate provides an interesting example and facilitates a more direct comparison as the sequence between the three paralogs (GluA2–4) is particularly well conserved in amniotic vertebrates (Figure 4A and Supplementary Figure S6). Sequence recognition is essential for Adar2 binding via two double-stranded
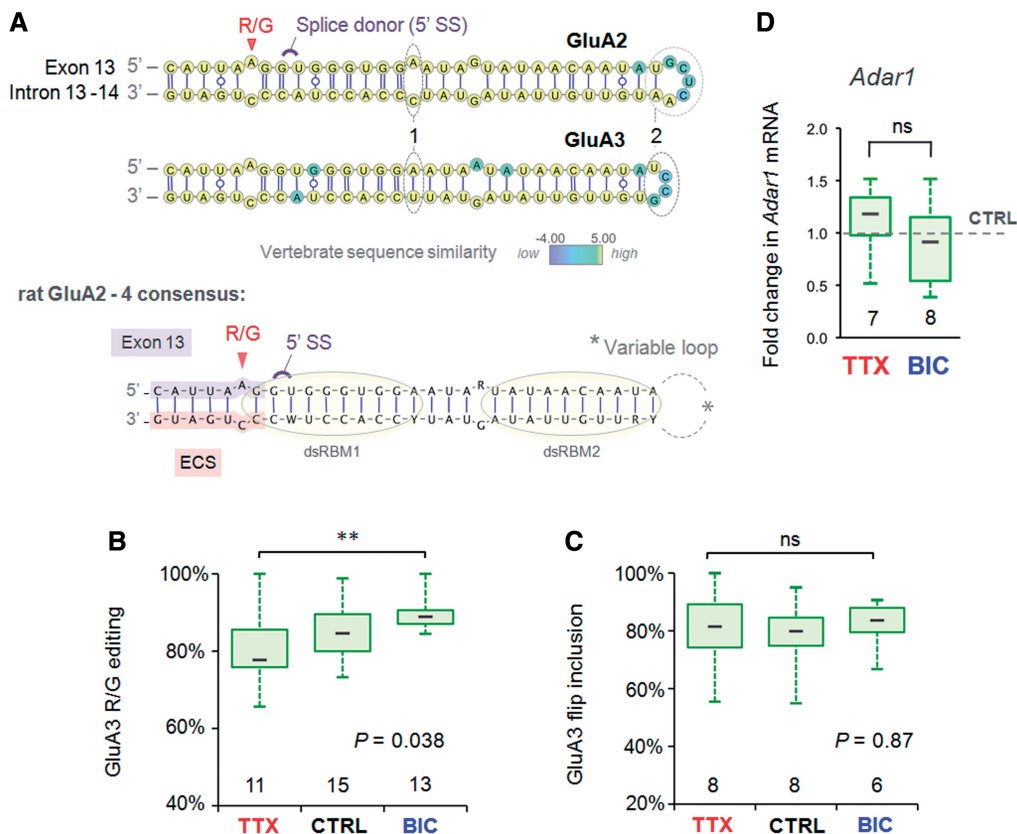
Figure 4. Comparison of activity-dependent R/G site regulation and substrate properties between AMPA subunit paralogs. (**A**) Top: the predicted common secondary structure (γ-centroid estimator) of the GluA2 and 3 pre-mRNA encompassing the R/G site for 10 vertebrate species (Supplementary Table S1 and Supplementary Figure S6) mapped onto the rat sequences. Base pairs are rendered according to the Leontis/Westhof (LW) nomenclature. The splice donor site (5′ SS) and editing sites are annotated in violet and red, respectively. Base positions are color-coded according to vertebrate sequence similarity (see color map), thus yellow base positions are completely conserved. Note the mismatch (1) and the longer loop sequence (2) distinguishing GluA2 from the GluA3 R/G editing substrate. Bottom: the consensus structure of the three rat paralogs of the GluA2–4 R/G editing substrates. Lilac highlight = exon sequence; salmon highlight = R/G site ECS. The putative binding sites of the two dsRBMs of Adar2 are illustrated with yellow circles. (**B**) Changes in R/G editing of GluA3 show regulation by an activity similar to GluA2, albeit to a lesser extent. The number at the base of each plot is the number of slices. The P-value is derived from the Kruskal–Wallis ANOVA test statistic and the asterices summarize the results of Dunn's post-tests: $**P < 0.01$. (**C**) The abundance of GluA3 flip splice variant as a fraction of total subunit mRNA expressed in CA1 is plotted for the different drug treatments. Quantification of splice variants is determined from mean peak height ratios for the first alternatively spliced nucleotide positions. GluA3 flip/flop splicing is invariant across drug treatments. (**D**) The fold change in CA1 mRNA levels of *Adar1* relative to the mean of intra-PCR run CTRL treatments is plotted (box and whisker) for the (48 h) drug treatments. *Adar1* expression was normalized to the endogenous house keeping gene *Gapdh*. *Adar1* expression was comparable between CTRL and TTX. The two-tailed P-value and asterisks are derived from the Mann–Whitney U-test statistic, $P =$ ns.

RNA-binding motifs (dsRBMs) (Figure 4A, bottom) (55,56). Nevertheless, GluA2 (Figure 1C and D) and GluA4 (data not shown) show bi-directional regulation, whereas GluA3 editing does not; editing at this site is near saturation under control conditions and exhibits only slightly reduced editing post-TTX (Figure 4B). A clear difference between the three RNA substrates maps to the terminal loop sequence, which is contacted in a sequence-specific manner by dsRBM2 of Adar2 (Figure 4A and Supplementary Figure S6) (56). This shorter GluA3 loop sequence or more distal intronic structures (57,58) could stabilize the RNA structure making it a better substrate (56,59). Alternatively, the higher editing levels at this site could be due to editing by the related editase, Adar1. Consistent with this, Adar1 levels did not change significantly between the treatments (Figure 4C) and Adar1-specific sites were not recoded in a

bi-directional fashion. Therefore, differences in intronic sequence appear to specify the substrate-specific activity-driven editing by Adar2. As noted above for GluA2, in addition to the heightened R/G editing, inclusion of the flip exon was markedly more pronounced in GluA3.

Flip/flop splicing and R/G editing are expressed in a gradient across CA1

In mouse CA1 flop isoforms predominate (37), contrasting with rat CA1 where both splice variants, flip and flop are co-expressed (Figure 1C). As stated above, R/G editing followed this segregation between the two subfields (for GluA2; Figure 1F and Supplementary Figure S2). Unexpectedly, we found that transcript isoform distribution in rat CA1 was not homogeneous but rather was expressed in a graded fashion (Figure 5A and E): R/G-edited GluA2 is more abundant at the CA3 to CA1 border
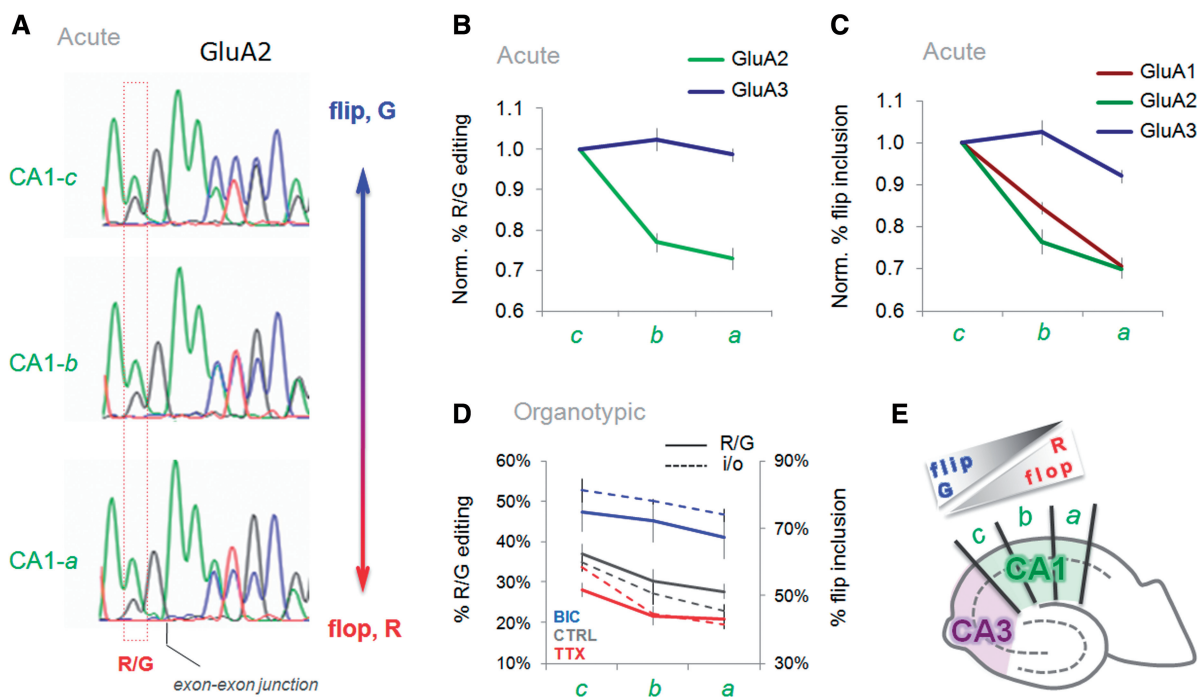
Figure 5. GluA subunit RNA processing is expressed in a gradient across CA1. (**A**) Sequence traces of PCR-amplified GluA2 from acutely dissected CA1 segments (CA1-c, -b, -a) document a gradual reduction of the flip exon and R/G editing towards the subiculum. (**B**) Quantification of the peak heights from sequence chromatograms is summarized in line plots. The plot documents normalized levels of R/G editing for the GluA2 and GluA3 transcripts in acutely dissected CA1 (CA1-c to -a). Results are normalized to levels of R/G editing in CA1-c. (**C**) Line plot indicating a gradual change of flip/flop splicing for all three GluA paralogs in acutely dissected CA1. Results are normalized to levels of flip in CA1-c. (**D**) Line plot summarizing R/G editing (solid line) and i/o splicing (dashed line) data for CTRL (gray) and drug-treated, TTX (red), BIC (blue) organotypic slices. The left *y*-axis represents the percentage of R/G editing, the right *y*-axis represents percentage flip exon inclusion. (**E**) Schematic of a hippocampal slice, depicting the two major subfields, CA3 (purple) and CA1 (green). CA1 subsegments (CA1-c to -a) are indicated. As indicated, levels of flip and editing diminish toward the subiculum at the expense of flop.

(CA1-c) but gradually diminishes towards the subiculum subfield where unedited GluA2 transcripts predominate (Figure 5A and B). This was substrate-specific and was less apparent for the more efficiently edited GluA3 RNA (Figure 5B). In addition to editing, i/o splicing followed this gradient: flip isoforms were highest in CA1 proximal to CA3 (CA1-c) but tapered off towards the subiculum (CA1-a; Figure 5C and E). An even steeper drop was observed for GluA1 splicing (see 'Discussion' section; Figure 5C). Together, these findings provide a further indication for a mechanistic link between these two RNA processing events. A gradient was also evident in organotypic hippocampal cultures (Figure 5D). Overall levels of flip isoforms were reduced after chronic TTX treatment (or increased after chronic BIC), the gradient however was preserved relative to untreated controls (Figure 1D). These results reveal a surprisingly dynamic and complex regulation of alternative RNA processing in the AMPAR LBD. How these findings impact on AMPAR biogenesis and gating kinetics, and in turn, on information processing in the hippocampal circuitry remains to be determined.

DISCUSSION

In this study we show that A-to-I RNA editing is subject to regulation, analogous to alternative splicing. This control will permit fine-tuning of editing targets, i.e. proteins shaping neuronal signaling and thus neuronal communication in a spatiotemporal fashion. Use of an intact model circuitry revealed that editing is regulated in a cell- and subfield-selective manner, providing an additional layer of control. Recoding was also substrate-specific and was linked to fluctuations in *Adar2* mRNA levels. Finally, editing at the GluA2 R/G site was reversible and correlated with alternative i/o splicing, and is therefore expected to impact on multiple aspects of AMPAR-mediated neurotransmission (17,18,24,37).

We treated neurons chronically to alter network activity, which resulted in a gradual change of editing over time (TTX $t_{1/2}$ ~11 h; Figure 2A). This paradigm contrasts with acute depolarization protocols that have been employed more commonly to induce changes in alternative splicing (20,60). Chronic TTX and BIC treatments alter AMPAR signaling in a homeostatic manner, i.e. TTX silencing upregulates the AMPAR response component (thereby increasing synaptic gain), whereas chronic BIC results in the opposite (40). How neurons regulate this receptor redistribution is not fully understood, although the GluA2 subunit appears to be centrally involved (39,61,62). This subunit controls Ca^{2+} flux through AMPARs, which is pivotal to brain physiology and pathology [e.g. (9,10,12)]. The finding that alternative splicing (21) and R/G editing dynamically respond to

fluctuations in activity will have consequences for AMPAR subunit assembly (23,63), which in addition to altering channel properties at synapses could have secondary effects on trafficking to synapses. Besides impacting ER exit and endocytic traffic, AMPARs of different stoichiometries have the capacity to be targeted to different dendritic regions within individual neurons (64).

An interplay between the R/G site and i/o splicing has been addressed in earlier studies *in vitro* (65) and it was shown that GluA2 R/G editing represses splicing of the proximal (flop) intron (42). Here, we extend this relationship to the endogenous transcript in neuronal tissue. A correlation between R/G editing and the downstream flip exon was apparent in hippocampal subfields, which followed activity manipulations in a bi-directional and reversible manner. Editing is expected to weaken the splice donor site. Because editing and splicing occur, co-transcriptional (66) RNA polymerase II processivity might be a decisive factor in this regulation (67). This idea is supported by the fact that in the GluA1 transcript, which harbors a stronger splice donor site in exon 13 (score: 11.08; see 'Materials and Methods' section) than GluA2, splicing to the adjacent flop exon is more prominent. In fact, a steeper drop of GluA1 flip, relative to GluA2 flip, is seen across the gradient in CA1 (Figure 5C). Accordingly, Adar2, which is under complex cellular control (48,68) and responded to the activity treatments in a bi-directional fashion (Figure 3A), might contribute to regulating i/o splicing by weakening the exon 13 splice donor.

While this manuscript was in preparation, a related study that used dissociated cortical neurons, described activity-regulated A-to-I RNA editing (69). The authors utilized high-throughput Illumina sequencing platforms to assess genome-wide changes in editing in response to acute and chronic changes in activity. This article provides a complementary study to the work described here. Together, these data suggest that RNA editing by ADARs provides a powerful and dynamic regulation of neuronal communication.

SUPPLEMENTARY DATA

Supplementary Data are available at NAR Online: Supplementary Tables 1 and 2, Supplementary Figures 1–6, Supplementary Methods and Supplementary Reference [70].

ACKNOWLEDGEMENTS

We thank the MRC LMB Biomedical Facility for help with animal work and the LMB workshop for help with various pieces of specific equipment. We thank Jill Hanby and Jernej Ule for critically reading of the manuscript.

FUNDING

Conflict of interest statement. None declared.

REFERENCES

1. Bass,B.L. (2002) RNA editing by adenosine deaminases that act on RNA. *Annu. Rev. Biochem.*, **71**, 817–846.
2. Jepson,J.E. and Reenan,R.A. (2008) RNA editing in regulating gene expression in the brain. *Biochim. Biophys. Acta*, **1779**, 459–470.
3. Hundley,H.A. and Bass,B.L. (2012) ADAR editing in double-stranded UTRs and other noncoding RNA sequences. *Trends Biochem. Sci.*, **35**, 377–383.
4. Peng,Z., Cheng,Y., Tan,B.C., Kang,L., Tian,Z., Zhu,Y., Zhang,W., Liang,Y., Hu,X., Tan,X. *et al.* (2012) Comprehensive analysis of RNA-Seq data reveals extensive RNA editing in a human transcriptome. *Nat. Biotechnol.*, **30**, 253–260.
5. Paul,M.S. and Bass,B.L. (1998) Inosine exists in mRNA at tissue-specific levels and is most abundant in brain mRNA. *EMBO J.*, **17**, 1120–1127.
6. Hoopengardner,B., Bhalla,T., Staber,C. and Reenan,R. (2003) Nervous system targets of RNA editing identified by comparative genomics. *Science*, **301**, 832–836.
7. Tariq,A. and Jantsch,M.F. (2012) Transcript diversification in the nervous system: A to I RNA editing in CNS function and disease development. *Front. Neurosci.*, **6**, 99.
8. Palladino,M.J., Keegan,L.P., O'Connell,M.A. and Reenan,R.A. (2000) A-to-I pre-mRNA editing in Drosophila is primarily involved in adult nervous system function and integrity. *Cell*, **102**, 437–449.
9. Seeburg,P.H. and Hartner,J. (2003) Regulation of ion channel/neurotransmitter receptor function by RNA editing. *Curr. Opin. Neurobiol.*, **13**, 279–283.
10. Maas,S., Kawahara,Y., Tamburro,K.M. and Nishikura,K. (2006) A-to-I RNA editing and human disease. *RNA Biol.*, **3**, 1–9.
11. Rosenthal,J.J. and Seeburg,P.H. (2012) A-to-I RNA editing: effects on proteins key to neural excitability. *Neuron*, **74**, 432–439.
12. Traynelis,S.F., Wollmuth,L.P., McBain,C.J., Menniti,F.S., Vance,K.M., Ogden,K.K., Hansen,K.B., Yuan,H., Myers,S.J., Dingledine,R. *et al.* (2010) Glutamate receptor ion channels: structure, regulation, and function. *Pharmacol. Rev.*, **62**, 405–496.
13. Seeburg,P.H. (1996) The role of RNA editing in controlling glutamate receptor channel properties. *J. Neurochem.*, **66**, 1–5.
14. Greger,I.H., Khatri,L., Kong,X. and Ziff,E.B. (2003) AMPA receptor tetramerization is mediated by Q/R editing. *Neuron*, **40**, 763–774.
15. Sommer,B., Kohler,M., Sprengel,R. and Seeburg,P.H. (1991) RNA editing in brain controls a determinant of ion flow in glutamate-gated channels. *Cell*, **67**, 11–19.
16. Feldmeyer,D., Kask,K., Brusa,R., Kornau,H.C., Kolhekar,R., Rozov,A., Burnashev,N., Jensen,V., Hvalby,O., Sprengel,R. *et al.* (1999) Neurological dysfunctions in mice expressing different levels of the Q/R site-unedited AMPAR subunit GluR-B. *Nat. Neurosci.*, **2**, 57–64.
17. Lomeli,H., Mosbacher,J., Melcher,T., Hoger,T., Geiger,J.R., Kuner,T., Monyer,H., Higuchi,M., Bach,A. and Seeburg,P.H. (1994) Control of kinetic properties of AMPA receptor channels by nuclear RNA editing. *Science*, **266**, 1709–1713.
18. Greger,I.H., Akamine,P., Khatri,L. and Ziff,E.B. (2006) Developmentally regulated, combinatorial RNA processing modulates AMPA receptor biogenesis. *Neuron*, **51**, 85–97.
19. Li,Q., Lee,J.A. and Black,D.L. (2007) Neuronal regulation of alternative pre-mRNA splicing. *Nat. Rev. Neurosci.*, **8**, 819–831.
20. Xie,J. and Black,D.L. (2001) A CaMK IV responsive RNA element mediates depolarization-induced alternative splicing of ion channels. *Nature*, **410**, 936–939.

21. Penn,A.C., Balik,A., Wozny,C., Cais,O. and Greger,I.H. (2012) Activity-mediated AMPA receptor remodeling, driven by alternative splicing in the ligand-binding domain. *Neuron*, **76**, 503–510.

22. Coleman,S.K., Möykkynen,T., Cai,C., von Ossowski,L., Kuismanen,E., Korpi,E.R. and Keinänen,K. (2006) Isoform-specific early trafficking of AMPA receptor flip and flop variants. *J. Neurosci.*, **26**, 11220–11229.

23. Coleman,S.K., Möykkynen,T., Hinkkuri,S., Vaahtera,L., Korpi,E.R., Pentikäinen,O.T. and Keinänen,K. (2010) Ligand-binding domain determines endoplasmic reticulum exit of AMPA receptors. *J. Biol Chem.*, **285**, 36032–36039.

24. Greger,I.H., Ziff,E.B. and Penn,A.C. (2007) Molecular determinants of AMPA receptor subunit assembly. *Trends Neurosci.*, **30**, 407–416.

25. Penn,A.C., Williams,S.R. and Greger,I.H. (2008) Gating motions underlie AMPA receptor secretion from the endoplasmic reticulum. *EMBO J.*, **27**, 3056–3068.

26. Liu,Y. and Samuel,C.E. (1999) Editing of glutamate receptor subunit B pre-mRNA by splice-site variants of interferon-inducible double-stranded RNA-specific adenosine deaminase ADAR1. *J. Biol. Chem.*, **274**, 5070–5077.

27. Gahwiler,B.H. (1981) Organotypic monolayer cultures of nervous tissue. *J. Neurosci. Methods*, **4**, 329–342.

28. Ge,B., Gurd,S., Gaudin,T., Dore,C., Lepage,P., Harmsen,E., Hudson,T.J. and Pastinen,T. (2005) Survey of allelic expression using EST mining. *Genome Res.*, **15**, 1584–1591.

29. Goodman,L.A. (1965) On simultaneous confidence intervals for multinomial proportions. *Technometrics*, **7**, 247–254.

30. Altschul,S.F., Madden,T.L., Schaffer,A.A., Zhang,J., Zhang,Z., Miller,W. and Lipman,D.J. (1997) Gapped BLAST and PSI-BLAST: a new generation of protein database search programs. *Nucleic Acids Res.*, **25**, 3389–3402.

31. Birney,E., Andrews,T.D., Bevan,P., Caccamo,M., Chen,Y., Clarke,L., Coates,G., Cuff,J., Curwen,V., Cutts,T. *et al.* (2004) An overview of Ensembl. *Genome Res.*, **14**, 925–928.

32. Kent,W.J. (2002) BLAT–the BLAST-like alignment tool. *Genome Res.*, **12**, 656–664.

33. Venkatesh,B., Kirkness,E.F., Loh,Y.H., Halpern,A.L., Lee,A.P., Johnson,J., Dandona,N., Viswanathan,L.D., Tay,A., Venter,J.C. *et al.* (2007) Survey sequencing and comparative analysis of the elephant shark (Callorhinchus milii) genome. *PLoS Biol.*, **5**, e101.

34. Katoh,K., Kuma,K., Miyata,T. and Toh,H. (2005) Improvement in the accuracy of multiple sequence alignment program MAFFT. *Genome Inform.*, **16**, 22–33.

35. Hamada,M., Sato,K. and Asai,K. (2011) Improving the accuracy of predicting secondary structure for aligned RNA sequences. *Nucleic Acids Res.*, **39**, 393–402.

36. Darty,K., Denise,A. and Ponty,Y. (2009) VARNA: Interactive drawing and editing of the RNA secondary structure. *Bioinformatics*, **25**, 1974–1975.

37. Sommer,B., Keinanen,K., Verdoorn,T.A., Wisden,W., Burnashev,N., Herb,A., Kohler,M., Takagi,T., Sakmann,B. and Seeburg,P.H. (1990) Flip and flop: a cell-specific functional switch in glutamate-operated channels of the CNS. *Science*, **249**, 1580–1585.

38. Witter,M.P., Wouterlood,F.G., Naber,P.A. and Van Haeften,T. (2000) Anatomical organization of the parahippocampal-hippocampal network. *Ann. NY Acad. Sci.*, **911**, 1–24.

39. Turrigiano,G.G. (2008) The self-tuning neuron: synaptic scaling of excitatory synapses. *Cell*, **135**, 422–435.

40. Turrigiano,G.G., Leslie,K.R., Desai,N.S., Rutherford,L.C. and Nelson,S.B. (1998) Activity-dependent scaling of quantal amplitude in neocortical neurons. *Nature*, **391**, 892–896.

41. Fisahn,A., Pike,F.G., Buhl,E.H. and Paulsen,O. (1998) Cholinergic induction of network oscillations at 40 Hz in the hippocampus in vitro. *Nature*, **394**, 186–189.

42. Schoft,V.K., Schopoff,S. and Jantsch,M.F. (2007) Regulation of glutamate receptor B pre-mRNA splicing by RNA editing. *Nucleic Acids Res.*, **35**, 3723–3732.

43. Gallo,A., Keegan,L.P., Ring,G.M. and O'Connell,M.A. (2003) An ADAR that edits transcripts encoding ion channel subunits functions as a dimer. *EMBO J.*, **22**, 3421–3430.

44. Valente,L. and Nishikura,K. (2007) RNA binding-independent dimerization of adenosine deaminases acting on RNA and dominant negative effects of nonfunctional subunits on dimer functions. *J. Biol. Chem.*, **282**, 16054–16061.

45. Higuchi,M., Maas,S., Single,F.N., Hartner,J., Rozov,A., Burnashev,N., Feldmeyer,D., Sprengel,R. and Seeburg,P.H. (2000) Point mutation in an AMPA receptor gene rescues lethality in mice deficient in the RNA-editing enzyme ADAR2. *Nature*, **406**, 78–81.

46. Wang,Q., Khillan,J., Gadue,P. and Nishikura,K. (2000) Requirement of the RNA editing deaminase ADAR1 gene for embryonic erythropoiesis. *Science*, **290**, 1765–1768.

47. Lein,E.S., Hawrylycz,M.J., Ao,N., Ayres,M., Bensinger,A., Bernard,A., Boe,A.F., Boguski,M.S., Brockway,K.S., Byrnes,E.J. *et al.* (2007) Genome-wide atlas of gene expression in the adult mouse brain. *Nature*, **445**, 168–176.

48. Feng,Y., Sansam,C.L., Singh,M. and Emeson,R.B. (2006) Altered RNA editing in mice lacking ADAR2 autoregulation. *Mol. Cell. Biol.*, **26**, 480–488.

49. Rueter,S.M., Dawson,T.R. and Emeson,R.B. (1999) Regulation of alternative splicing by RNA editing. *Nature*, **399**, 75–80.

50. Gurevich,I., Englander,M.T., Adlersberg,M., Siegal,N.B. and Schmauss,C. (2002) Modulation of serotonin 2C receptor editing by sustained changes in serotonergic neurotransmission. *J. Neurosci.*, **22**, 10529–10532.

51. Hideyama,T., Yamashita,T., Aizawa,H., Tsuji,S., Kakita,A., Takahashi,H. and Kwak,S. (2012) Profound downregulation of the RNA editing enzyme ADAR2 in ALS spinal motor neurons. *Neurobiol. Dis.*, **45**, 1121–1128.

52. Hideyama,T., Yamashita,T., Suzuki,T., Tsuji,S., Higuchi,M., Seeburg,P.H., Takahashi,R., Misawa,H. and Kwak,S. (2010) Induced loss of ADAR2 engenders slow death of motor neurons from Q/R site-unedited GluR2. *J. Neurosci.*, **30**, 11917–11925.

53. Peng,P.L., Zhong,X., Tu,W., Soundarapandian,M.M., Molner,P., Zhu,D., Lau,L., Liu,S., Liu,F. and Lu,Y. (2006) ADAR2-dependent RNA editing of AMPA receptor subunit GluR2 determines vulnerability of neurons in forebrain ischemia. *Neuron*, **49**, 719–733.

54. Penn,A.C., Balik,A. and Greger,I.H. (2012) Steric antisense inhibition of AMPA receptor Q/R editing reveals tight coupling to intronic editing sites and splicing. *Nucleic Acids Res.*, **41**, 1113–1123.

55. Dawson,T.R., Sansam,C.L. and Emeson,R.B. (2004) Structure and sequence determinants required for the RNA editing of ADAR2 substrates. *J. Biol. Chem.*, **279**, 4941–4951.

56. Stefl,R., Oberstrass,F.C., Hood,J.L., Jourdan,M., Zimmermann,M., Skrisovska,L., Maris,C., Peng,L., Hofr,C., Emeson,R.B. *et al.* (2010) The solution structure of the ADAR2 dsRBM-RNA complex reveals a sequence-specific readout of the minor groove. *Cell*, **143**, 225–237.

57. Aruscavage,P.J. and Bass,B.L. (2000) A phylogenetic analysis reveals an unusual sequence conservation within introns involved in RNA editing. *RNA*, **6**, 257–269.

58. Daniel,C., Veno,M.T., Ekdahl,Y., Kjems,J. and Ohman,M. (2012) A distant cis acting intronic element induces site-selective RNA editing. *Nucleic Acids Res.*, **40**, 9876–9886.

59. Stefl,R. and Allain,F.H. (2005) A novel RNA pentaloop fold involved in targeting ADAR2. *RNA*, **11**, 592–597.

60. Lee,J.A., Xing,Y., Nguyen,D., Xie,J., Lee,C.J. and Black,D.L. (2007) Depolarization and CaM kinase IV modulate NMDA receptor splicing through two essential RNA elements. *PLoS Biol.*, **5**, e40.

61. Gainey,M.A., Hurvitz-Wolff,J.R., Lambo,M.E. and Turrigiano,G.G. (2009) Synaptic scaling requires the GluR2 subunit of the AMPA receptor. *J. Neurosci.*, **29**, 6479–6489.

62. Pozo,K. and Goda,Y. (2010) Unraveling mechanisms of homeostatic synaptic plasticity. *Neuron*, **66**, 337–351.

63. Brorson,J.R., Li,D. and Suzuki,T. (2004) Selective expression of heteromeric AMPA receptors driven by flip-flop differences. *J. Neurosci.*, **24**, 3461–3470.

64. Toth,K. and McBain,C.J. (1998) Afferent-specific innervation of two distinct AMPA receptor subtypes on single hippocampal interneurons. *Nat. Neurosci.*, **1**, 572–578.

65. Bratt,E. and Ohman,M. (2003) Coordination of editing and splicing of glutamate receptor pre-mRNA. *RNA*, **9**, 309–318.

66. Ryman,K., Fong,N., Bratt,E., Bentley,D.L. and Ohman,M. (2007) The C-terminal domain of RNA Pol II helps ensure that editing precedes splicing of the GluR-B transcript. *RNA*, **13**, 1071–1078.

67. de la Mata,M., Munoz,M.J., Allo,M., Fededa,J.P., Schor,I.E. and Kornblihtt,A.R. (2011) RNA polymerase II elongation at the crossroads of transcription and alternative splicing. *Genet. Res. Int.*, **2011**, 309865.

68. Marcucci,R., Brindle,J., Paro,S., Casadio,A., Hempel,S., Morrice,N., Bisso,A., Keegan,L.P., Del Sal,G. and O'Connell,M.A. (2011) Pin1 and WWP2 regulate GluR2 Q/R site RNA editing by ADAR2 with opposing effects. *EMBO J.*, **30**, 4211–4222.

69. Sanjana,N.E., Levanon,E.Y., Hueske,E.A., Ambrose,J.M. and Li,J.B. (2012) Activity-dependent A-to-I RNA editing in rat cortical neurons. *Genetics*, **192**, 281–287.

70. Higuchi,M., Single,F.N., Kohler,M., Sommer,B., Sprengel,R. and Seeburg,P.H. (1993) RNA editing of AMPA receptor subunit GluR-B: a base-paired intron-exon structure determines position and efficiency. *Cell*, **75**, 1361–1370.